Digital Object Identifier (DOI): 10.1109/IECON.2015.7392223

41st Annual Conference of the IEEE Industrial Electronics Society, Yokohama, Japan, 2015

Resonance damping in a smart transformer-based microgrid

Zhi-Xiang Zou
Marco Liserre
Zheng Wang
Ming Cheng
Shouting Fan

Suggested Citation

Z. Zou, M. Liserre, Z. Wang, M. Cheng and S. Fan, "Resonance damping in a smart transformer-based microgrid," *41st Annual Conference of the IEEE Industrial Electronics Society*, Yokohama, 2015, pp. 000956-000964.

Resonance Damping in a Smart Transformer-based Microgrid

Zhi-Xiang Zou, Marco Liserre
Chair of Power Electronics
Christian-Albrechts-Universität zu Kiel
Kiel 24143, Germany
zz@tf.uni-kiel.de, ml@tf.uni-kiel.de

Zheng Wang, Ming Cheng, Shouting Fan
School of Electrical Engineering
Southeast University
Nanjing 210096, China
zwang@seu.edu.cn, mcheng@seu.edu.cn,
fanshouting1988@126.com

***Abstract*—Compared with the traditional microgrid, a smart transformer (ST)-based microgrid shows advantages in terms of higher efficiency, increased hosting capacity, and enhanced reliability. However, this novel microgrid presents challenges because of the complex resonances within the system and the interactions between ST and power converter-based distributed energy resources (DERs). Both the ST and DERs might be severely affected by each other and leads to performance degradation and system instability. To solve these problems, this paper first develops equivalent circuits of a ST-based microgrid. Then, the resonance and interaction problems are investigated based on the equivalent circuits. The active damping method is used to fully address the resonance issue and mitigate the coupling effects. To guarantee superior performance, this paper also designs high-performance control strategies for both the ST and DERs. Simulation and experimental results are provided to verify the validity of the proposed control strategy.**

Keywords—microgrid; smart transformer (ST); resonance; active damping; repetitive control

I. INTRODUCTION

The increasing spread installation of DERs challenges the hosting capacity of distribution network and microgrids. In Germany for example, the share of electricity produced from DERs was about 30% in the first half of 2014. The government is working towards an ambitious plan that aims to achieve 80% renewable generation (most of them are DERs) by 2050 [1]. In addition, large amount of electric vehicles (EVs) along with the Vehicle-to-Grid (V2G) technology will be a promising alternative combined into the microgrids in the very near future [2]. These distributed devices are likely to impose severe problems on the existing microgrids in terms of voltage surge, line congestion, harmonic issue, and decreased stability margin [3-5]. These problems have been recognized by researchers in literature, but unfortunately most of the proposed approaches are only effective in some specific scenarios. More importantly, these distributed devices will impose a heavier burden on both the Microgrid Central Controller (MGCC) and the Distribution Network Operator (DNO). It is becoming more and more difficult to handle the overall microgrid as a whole controllable entity.

On the other hand, the next-generation microgrid is expected to deal with various kinds of DERs as well as EVs and controllable loads which usually are characterized with different voltage levels, voltage types (DC/AC), frequency, power rating, and power quality requirements. In this sense, a microgrid should contain various standard "plug-and-play" interfaces to ensure various distributed devices can be easily coupled into the network and achieve efficient power exchange among different types of subordinate grids [6]. Within the context of smart grid, microgrids are conjectured to be capable of full visibility and controllability of all the distributed devices. In this way, the microgrid is likely to optimize the power flow and regulate the node voltage profile in real time. Further, the microgrid can timely locate the fault and precisely trip the fault area, achieving brilliant reliability.

In this respect, the Smart Transformer (ST) concept is presented as one of the most promising alternatives that can exploit the full potential of existing microgrid and enhance the hosting capacity of DER and EV. The simplified configuration of a ST-based microgrid is shown in Fig. 1, where the ST is coupling with a variety of DERs, EVs, energy storage system (ESS), and different types of loads. It is important to stress that a ST is able to provide various types of electric interfaces for different distributed devices (for example, distributed devices require different voltage types, levels, frequencies and grid codes) [7]. Moreover, since the Medium Voltage (MV) side and the Low Voltage (LV) side are fully decoupled, the ST can provide superior voltage profile at the Point of Common Coupling (PCC) and therefore largely reduce the chance of unplanned islanding operation. In this paper, an AC microgrid is considered and different distributed devices are connected to the LVAC bus of the ST.

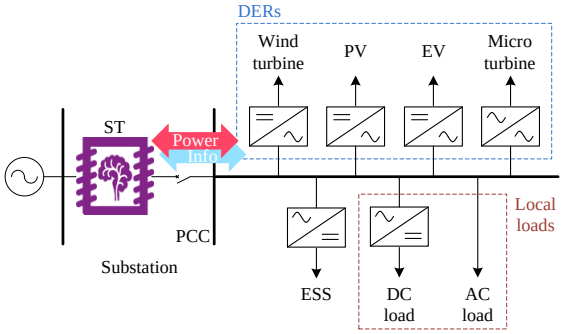

Fig. 1. ST-based microgrid concept

Although the ST-based microgrid shows great advantages in various aspects, it presents some challenges as well. One major concern is the resonance problem which is incurred by multiple paralleled power converters in the system. Previous research on microgrid resonances mainly focused on paralleled grid-connected inverters with *LCL* filter and damping methods. In [8], a passive circuit model was developed and trying to investigate the resonances and interactions among a large number of distributed power inverters. A more detailed model and transfer function matrix of *N*-paralleled PV inverters were presented in [9] which also analyzed resonance problem of paralleled inverters. The authors found that the equivalent grid impedance is increasing when more PV inverters are connected to the grid. On this basis, [10] further revealed the frequency-varying feature of resonances which are caused by inverters interaction and grid distortions. Recently, [11] also discussed the interactions of paralleled inverters and classified it as harmonic stability issue and employed impedance-based approach to model and analyze this issue. However, the ST-based microgrid is quite different from the previous scenarios in literature. From Fig. 1, the PCC voltage of AC network is provided by a DC/AC inverter with passive filters [12], thus the PCC voltage cannot be assumed as an ideal voltage source as that in the former analysis. New features and the interactions between the ST and DERs must be considered.

This paper aims at studying the resonance and interaction problem in a ST-based microgrid. An equivalent system model considering new features of ST is developed. The resonance and interaction as well as stability issues can be investigated by using two equivalent circuits which are derived from the equivalent model. To address these issues, active damping method can be used to alleviate the adverse effects and improve stability margin. Moreover, control designs are proposed for both the ST and DER inverters to guarantee a stiff voltage profile of PCC and high power quality DER currents. Simulations and experimental results from a laboratory prototype verify the effectiveness of our investigation and proposed control strategies.

II. Modeling of ST-based Microgrid

In a ST-based microgrid, the voltage profile of each node and power flow within the network can be regulated by modifying the injection of active and reactive power of each DER which is connected to the PCC. Various optimal algorithms have been proposed to provide explicit set-points for each distributed device in different microgrid scenarios. For instance, a centralized control scheme with voltage control and line congestion management functionalities has been proposed in [13] and adopted in a ST-based distribution network [14], providing improved ancillary services and performance. With this configuration, the ST LV side can be regarded as a voltage-controlled DC/AC inverter with an *LC* filter guaranteeing a stiff voltage profile at the PCC, while the connected DERs can be simplified as a set of paralleled current-controlled inverters with *LCL* filters interconnected through feeders. The simplified configuration of the ST-based microgrid is shown in Fig. 2(a). Since the main objective of this paper is to study the resonance and interaction problems between the ST and DERs, the front stages and intermediate energy conversion converters are ignored and replaced by the DC sources. Moreover, in this paper all the DER inverters as

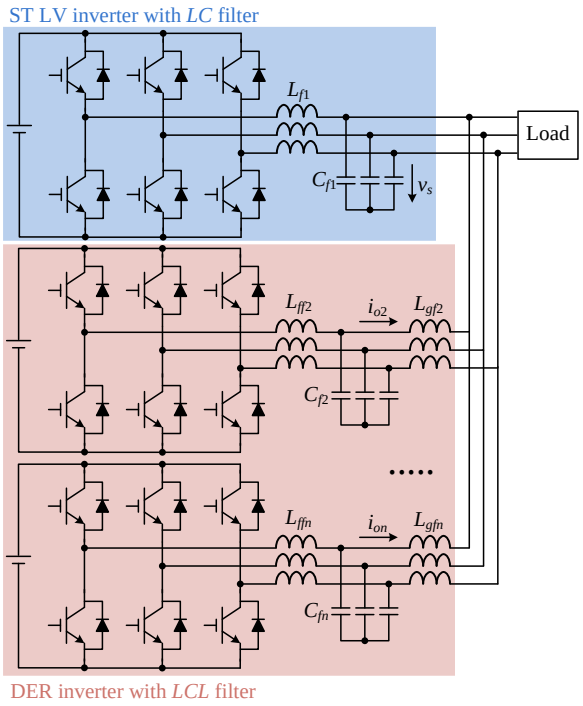

(a)

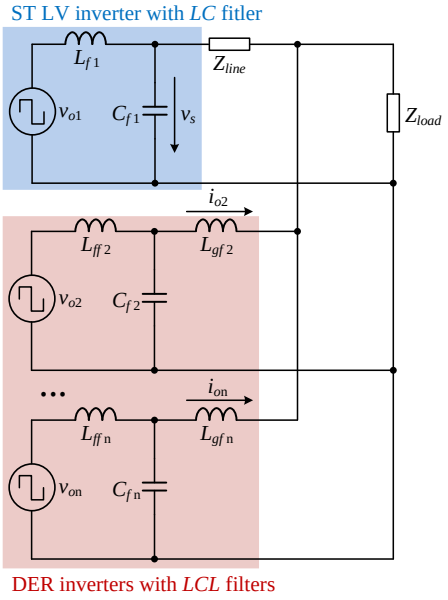

(b)

Fig. 2. Simplified model of a ST-based microgrid: (a) hardware configuration and (b) eqivalent system model

well as their *LCL* filters are assumed with same sort and thus the inverter parameters and filter values are identical (*e.g.* L_{ff2}= L_{ff3}=⋯= L_{ffn}= L_{ff}, L_{gf2}= L_{gf3}=⋯= L_{gfn}= L_{gf}, and C_{f2}= C_{f3}=⋯= C_{fn}= C_f). To well describe the resonance problem and interaction effects between ST and DERs, an equivalent system model is developed based on Fig. 2(a) and shown in Fig. 2(b), where Z_{line} is the line impedance between ST and PCC, and Z_{load} is the equivalent load impedance. From the equivalent model, it is easy to see that both the ST LV side voltage v_s and the DER output currents i_{ok} ($2 \le k \le n$) are excited by multiple inverter sources v_{ok} ($1 \le k \le n$). Here, the DERs are numbering from 2 to

n, thus the value of $n-1$ represents the number of DERs being connected to the PCC.

Based on the equivalent model, the dynamics of the simplified ST-based microgrid can be described as Eq. (1), where $\mathbf{v_{on}}$ is the input vector which represents the voltage outputs of the inverters v_{ok}; and $\mathbf{G(s)}$ is the matrix of the transfer functions, from the inverter sources (v_{ok}) to the control variables (v_s or i_{ok}). Since the parameters of all the DERs are equal, all the transfer functions from v_{o1} to i_{ok} are identical, and all the transfer functions from v_{ok} ($k \neq 1$) to v_s are identical as well. Hence, the non-diagonal elements of the first row and the first column of the matrix can be rewritten as that in Eq. (2).

$$\begin{pmatrix} v_s \\ i_{o2} \\ \cdots \\ i_{on} \end{pmatrix} = \mathbf{G(s)} \cdot \mathbf{v_{on}} = \begin{pmatrix} G_{11} & G_{12} & \cdots & G_{1n} \\ G_{21} & G_{22} & \cdots & G_{2n} \\ \cdots & \cdots & \cdots & \cdots \\ G_{n1} & G_{n2} & \cdots & G_{nn} \end{pmatrix} \cdot \begin{pmatrix} v_{o1} \\ v_{o2} \\ \cdots \\ v_{on} \end{pmatrix} \tag{1}$$

$$\begin{aligned} G_{12} &= G_{13} = \cdots = G_{1n} \\ G_{21} &= G_{31} = \cdots = G_{n1} \end{aligned} \tag{2}$$

A submatrix $\mathbf{G_i(s)}$ can be obtained by deleting the first row and the first column and it turns out to be a symmetric matrix, i.e. $\mathbf{G_i} = \mathbf{G_i}^{\mathrm{T}}$, in which all the diagonal elements and all the non-diagonal elements are identical, respectively. Therefore, $\mathbf{G_i(s)}$ can be rewritten as follows

$$\mathbf{G_i(s)} = \begin{pmatrix} G_{22} & G_{23} & \cdots & G_{2n} \\ G_{32} & G_{33} & \cdots & G_{3n} \\ \cdots & \cdots & \cdots & \cdots \\ G_{n2} & G_{n3} & \cdots & G_{nn} \end{pmatrix} = \begin{pmatrix} G_{22} & G_{23} & \cdots & G_{23} \\ G_{23} & G_{22} & \cdots & G_{23} \\ \cdots & \cdots & \cdots & \cdots \\ G_{23} & G_{23} & \cdots & G_{22} \end{pmatrix} \tag{3}$$

Substituting (2) and (3) into (1), we get

$$\begin{pmatrix} v_s \\ i_{o2} \\ \cdots \\ i_{on} \end{pmatrix} = \begin{pmatrix} G_{11} & G_{12} & \cdots & G_{12} \\ G_{21} & G_{22} & \cdots & G_{23} \\ \cdots & \cdots & \cdots & \cdots \\ G_{21} & G_{23} & \cdots & G_{22} \end{pmatrix} \cdot \begin{pmatrix} v_{o1} \\ v_{o2} \\ \cdots \\ v_{on} \end{pmatrix} \tag{4}$$

In order to calculate each element (i.e. transfer function) in the matrix $\mathbf{G(s)}$ of (4), two equivalent circuits in Fig. 3 can be obtained through the superposition theorem. The elements G_{11} and G_{21} can be calculated if all the DER inverter sources are supposed to be zero as shown in Fig. 3(a). Likewise, the elements G_{12}, G_{22}, and G_{23} can be calculated by supposing all the inverter sources to be zero except one of the DER inverter source v_{ok}, and the corresponding equivalent circuit is shown in Fig. 3(b). In these circuits, the same sort DER output filters are paralleled together, and thus $Z_{gfeq} = s{\cdot}L_{gf}/(n-1)$, $Z_{ffeq} = s{\cdot}L_{ff}/(n-1)$, $Z_{cfeq} = 1/(s{\cdot}L_{gf}\cdot(n-1))$, $Z_{gfeq}' = s{\cdot}L_{gf}/(n-2)$, $Z_{ffeq}' = s{\cdot}L_{ff}/(n-2)$, and $Z_{cfeq}' = 1/(s{\cdot}L_{gf}\cdot(n-2))$.

A. Transfer Functions of ST LV Side's Inverter

The diagonal element G_{11} can be considered as the transfer function from the ST inverter output voltage v_{o1} to the ST LV side voltage v_s, while the non-diagonal element G_{12} is the transfer function from one of the DER inverters output voltages v_{ok} to v_s. Specifically, G_{11} might be the transfer function of the

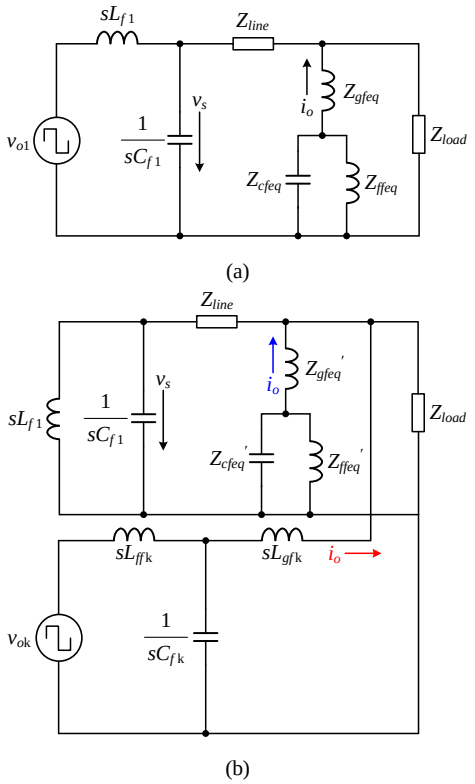

Fig. 3. Equivalent circuits: (a) $v_{o2} = 0$ and (b) $v_{o1} = 0$

LC filter if there is no DER connected to the PCC. G_{11} can be calculated by using the equivalent circuit of Fig. 3(a) and expressed as follows

$$G_{11} = \frac{v_s}{v_{o1}} = \frac{a_3 s^3 + a_2 s^2 + a_1 s + a_0}{b_5 s^5 + b_4 s^4 + b_3 s^3 + b_2 s^2 + b_1 s + b_0} \tag{5}$$

where

$$\begin{aligned} a_3 &= C_f L_{ff} L_{gf} (Z_{line} + Z_{load}) \\ a_2 &= (n-1) C_f L_{ff} Z_{line} Z_{load} \\ a_1 &= (L_{ff} + L_{gf})(Z_{line} + Z_{load}) \\ a_0 &= (n-1) Z_{line} Z_{load} \end{aligned}$$

and

$$\begin{aligned} b_5 &= C_f C_{f1} L_{f1} L_{ff} L_{gf} (Z_{line} + Z_{load}) \\ b_4 &= C_f L_{f1} L_{ff} L_{gf} + (n-1) C_f C_{f1} L_{f1} L_{ff} Z_{line} Z_{load} \\ b_3 &= (Z_{line} + Z_{load})(C_{f1} L_{f1} L_{ff} + C_{f1} L_{f1} L_{gf} C_f L_{ff} L_{gf}) + (n-1) C_f L_{f1} L_{ff} \\ b_2 &= (n-1)(C_{f1} L_{f1} Z_{line} Z_{load} + C_f L_{ff} Z_{line} Z_{load}) + L_{f1}(L_{ff} + L_{gf}) \\ b_1 &= (L_{ff} + L_{gf})(Z_{line} + Z_{load}) + (n-1) L_{f1} Z_{load} \\ b_0 &= (n-1) Z_{line} Z_{load} \end{aligned}$$

On the other hand, the non-diagonal element G_{12} can be calculated by using the equivalent circuit of Fig. 3(b) and the expression of G_{12} is given as follows

$$G_{12} = \frac{v_s}{v_{ok}} = \frac{(L_{f1} Z_{load}) s}{b_5 s^5 + b_4 s^4 + b_3 s^3 + b_2 s^2 + b_1 s + b_0} \tag{6}$$

The Bode diagrams of G_{11} with different n are shown in

Fig. 4(a), in which the value of $n-1$ indicates the number of DERs being connected to the PCC. As we can see, the connection of DERs introduces one additional pole and zero to the system and therefore arouses an additional resonance peak at its resonance frequency. To better investigate the resonance problem, the resonance peak aroused by the device itself is defined as internal resonance, while the resonance peak(s) aroused by the other devices are defined as external resonance(s). With the increasing of the DERs, both the external and internal resonance peaks shift towards the medium frequency range.

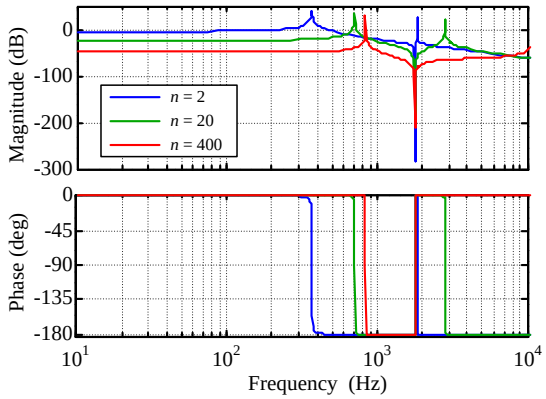

(a)

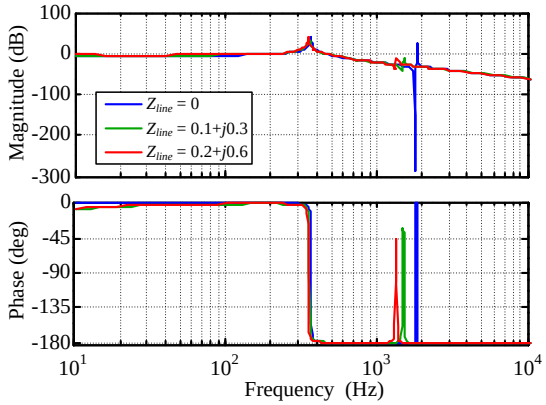

(b)

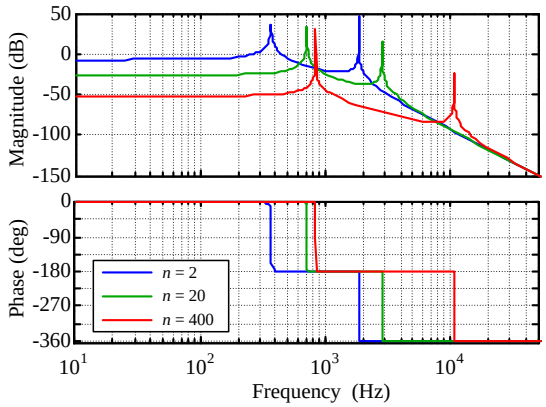

(c)

Fig. 4. Bode diagrams of ST-related transfer functions: (a) diagonal element G_{11} with different n, (b) G_{11} with different line impedances, and (c) non-diagonal elements G_{12}

Meanwhile, the impact of line impedance on the ST is also investigated and the Bode diagrams of G_{11} with different line impedances are shown in Fig. 4(b). It can be seen that the resonance peak introduced by the DERs can be well dampened with higher impedance value. This means the DERs would have insignificant effects on the ST LV side if they are installed far away from the ST.

On the other hand, the Bode diagrams of G_{12} with different n are shown in Fig. 5(c). When the DER number is relatively low, both the coupling effect and resonance issue are severe. However, with the increasing of DERs, the resonance peak of DERs can be largely attenuated and the amplitude of G_{12} could be maintained at the allowable low level. For example, when 399 DERs are connected to the PCC, the amplitude of G_{12} is less than −10dB within the whole frequency range except the resonance point of ST itself, which means the DER sources impose very limited coupling effects on the ST LV side voltage.

B. *Transfer Functions of DER Inverters*

For the DER output current i_{ok}, there are three types of elements in **G(s)**, which are G_{21}, G_{22}, and G_{23}. The first non-diagonal element G_{21} can be considered as the transfer function from the ST inverter output voltage v_{o1} to the DER output current i_{ok}. Based on the equivalent circuit of Fig. 3(a), the expression of G_{21} can be obtained as

$$G_{21}=\frac{i_{ok}}{v_{o1}}=-\frac{C_f L_{ff} Z_{load} s^2+Z_{load}}{b_5 s^5+b_4 s^4+b_3 s^3+b_2 s^2+b_1 s+b_0} \tag{7}$$

Likewise, the expression of G_{22} and G_{23} can be calculated based on the ancillary circuit of Fig. 3(b). G_{22} is the transfer function from one of the DER inverters output voltages v_{ok} to its output current (red arrow), while G_{22} is the transfer function from one of the DER inverters output voltages v_{ok} to the output current of another DER (blue arrow). The detailed expressions are illustrated in (8) and (9) as follows

$$G_{22}=\frac{i_{ok}}{v_{ok}}=\frac{b_5 s^5+d_4 s^4+d_3 s^3+d_2 s^2+d_1 s+d_0}{c_8 s^8+c_7 s^7+c_6 s^6+c_5 s^5+c_4 s^4+c_3 s^3+c_2 s^2+c_1 s} \tag{8}$$

where

$$c_8=C_f^2 C_{f1} L_{f1} L_{ff}^2 L_{gf}^2 (Z_{line}+Z_{load})$$

$$c_7=C_f^2 L_{f1} L_{ff}^2 L_{gf}^2+(n-1)C_f^2 C_{f1} L_{f1} L_{ff}^2 L_{gf} Z_{line} Z_{load}$$

$$c_6=(n-1)C_f^2 L_{f1} L_{ff}^2 L_{gf} Z_{load}+(Z_{line}+Z_{load})\cdot(C_f^2 L_{ff}^2 L_{gf}^2+2C_f C_{f1} L_{f1} L_{ff} L_{gf}(L_{ff}+L_{gf}))$$

$$c_5=2C_f L_{f1} L_{ff} L_{gf}(L_{ff}+L_{gf})+(n-1)Z_{line} Z_{load}(C_f^2 L_{ff}^2 L_{gf}+C_f C_{f1} L_{f1} L_{ff}^2+2C_f C_{f1} L_{f1} L_{ff} L_{gf})$$

$$c_4=C_{f1} L_{f1}(L_{ff}^2+L_{gf}^2)\cdot(Z_{line}+Z_{load})+2C_f L_{ff} L_{gf}(L_{ff}+L_{gf})\cdot(Z_{line}+Z_{load})+(n-1)C_f L_{f1} L_{ff} Z_{load}(L_{ff}+2L_{gf})+2C_{f1} L_{f1} L_{ff}\cdot L_{gf}(Z_{line}+Z_{load})$$

$$c_3=L_{f1}(L_{ff}+L_{gf})^2+(n-1)Z_{line} Z_{load}(C_f L_{ff}^2+C_{f1} L_{f1}(L_{ff}+L_{gf})+2C_f L_{ff} L_{gf})$$

$$c_2=(Z_{line}+Z_{load})\cdot(L_{ff}+L_{gf})^2+(n-1)\cdot(L_{ff}+L_{gf})L_{f1} Z_{load}$$

$$c_1 = (n-1)Z_{line}Z_{load}(L_{ff} + L_{gf})$$

and

$$d_4 = C_f L_{f1} L_{ff} (L_{gf} + (n-2) \cdot C_{f1} Z_{line} Z_{load})$$

$$d_3 = (Z_{line} + Z_{load}) \cdot (C_{f1} L_{f1} (L_{ff} + L_{gf}) + C_f L_{ff} L_{gf}) + (n-2) \cdot C_f L_{f1} L_{ff} Z_{load}$$

$$d_2 = L_{f1}(L_{ff} + L_{gf}) + (n-2) \cdot (C_{f1} L_{f1} + C_f L_{ff}) Z_{line} Z_{load}$$

$$d_1 = (L_{ff} + L_{gf}) \cdot (Z_{line} + Z_{load}) + (n-2) \cdot L_{f1} Z_{load}$$

$$d_0 = (n-2) \cdot Z_{line} Z_{load}$$

$$G_{23} = \frac{i_{ok}}{v_{oj}} = -\frac{e_4 s^4 + e_3 s^3 + e_2 s^2 + e_1 s + e_0}{c_8 s^8 + c_7 s^7 + c_6 s^6 + c_5 s^5 + c_4 s^4 + c_3 s^3 + c_2 s^2 + c_1 s} \quad (9)$$

where

$$e_4 = C_f C_{f1} L_{f1} L_{ff} Z_{line} Z_{load}$$

$$e_3 = C_f L_{f1} L_{ff} Z_{load}$$

$$e_2 = Z_{line} Z_{load} (C_{f1} L_{f1} + C_f L_{ff})$$

$$e_1 = L_{f1} Z_{load}$$

$$e_0 = Z_{line} Z_{load}$$

The Bode diagrams of G_{21} with different n are shown in Fig. 5(a). It is obviously to see that the ST LV side inverter will introduce an additional resonance peak into the overall system. With the increasing of the DERs, this resonance peak would be attenuated and shift towards the higher frequency range. The Bode diagrams of G_{22} and G_{23} with different n are shown in Fig. 5(b) and (c). In both diagrams, the external resonances and the coupling interactions will be further mitigated by increasing the number of DERs in the microgrid, while the internal resonances are always the same under different conditions so that necessary damping method is needed.

III. Control and Resonance Damping

A. Active Damping Analysis

The active damping methods including filter-based active damping and multiloop-based active damping have been applied to standalone and grid-connected inverter applications [15-16]. It shows effectiveness to resonance and is less sensitive to the parameter variations. In this paper, the multiloop-based active damping method is employed, which is to mimic the idea of passive damping through an inner feedback control loop. For inverters with *LC* or *LCL* filters, the inductor current and capacitor current inner-loop feedbacks are commonly used to maintain stability and alleviate adverse features caused by resonances.

To well analyze the open-loop features, the PWM block and the computation as well as the ADC block are considered as the $1.5T_s$ delay due to elaboration of the computation device (T_s) and to the PWM ($0.5T_s$), it can be expended by using Padé Approximant as following:

$$G_d(s) = e^{-1.5T_s s} \approx \frac{12 - 9T_s \cdot s + 2.25T_s^2 \cdot s^2}{12 + 9T_s \cdot s + 2.25T_s^2 \cdot s^2} \quad (10)$$

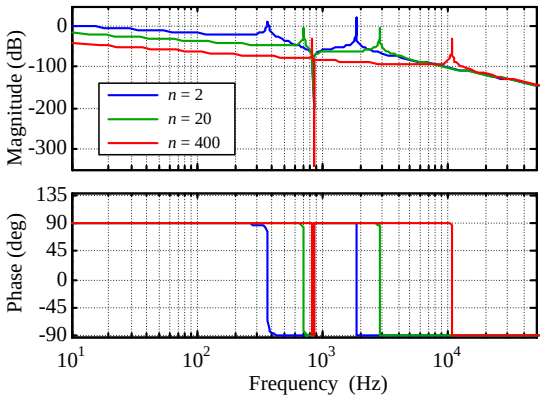

(a)

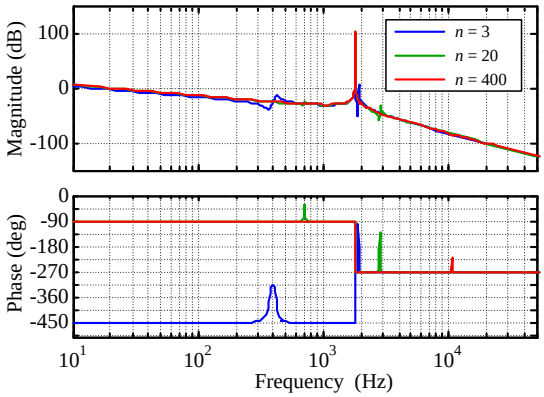

(b)

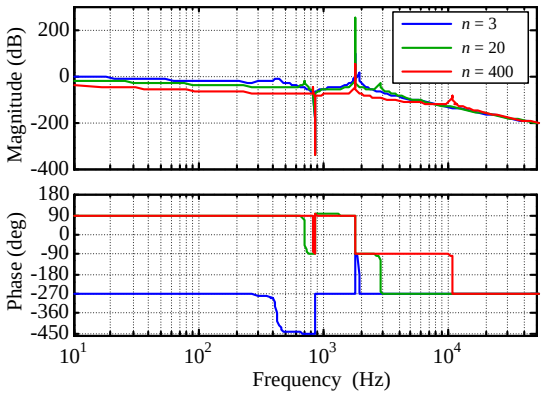

(c)

Fig. 5. Bode diagrams of DER-related transfer functions with different n: (a) non-diagonal element G_{21}, (b) diagonal element G_{22}, and (c) non-diagonal elements G_{23}

The detailed filter parameters of ST and DERs are shown in Table I. Fig. 6 compares the open-loop Bode diagrams for ST inverter with different inner-loop feedbacks. It is observed the external resonance peak caused by the DERs can be better damped by using capacitor current feedback when same inner gains are used, whereas the phase margins of both two feedbacks are still the same. With these considerations, the capacitor current feedback is utilized in the DER inverter with better damping effects, while the inductor current feedback is employed in the ST inverter to alleviate resonance as well as to limit the output power rating.

By using the inner-loops, the open-loop Bode diagram of G_{11} with active damping is shown in Fig. 7(a) as the red line. In

this study case, four DERs are connected to the PCC of microgrid and the inner-loop gains of both the ST and DERs are selected as 5. For comparison, the Bode diagrams of G_{11} without damping are also shown in Fig. 7(a) as the blue and green lines. Obviously, with effective damping, both the internal and external resonance peaks are fully eliminated. There is neither positive nor negative −180º crossing at the critical frequency, which indicates the stability condition is well fulfilled in this system.

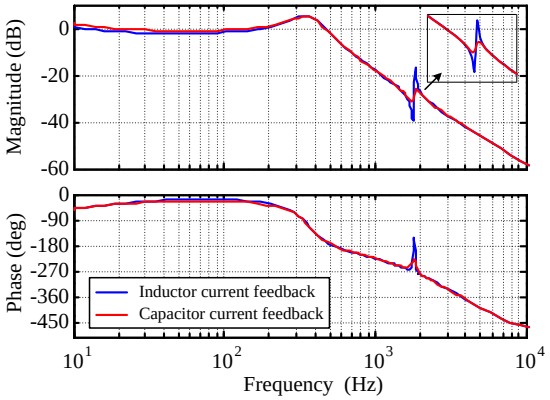

Fig. 6. Open-loop Bode diagrams of ST inverter with different multiloop active damping methods

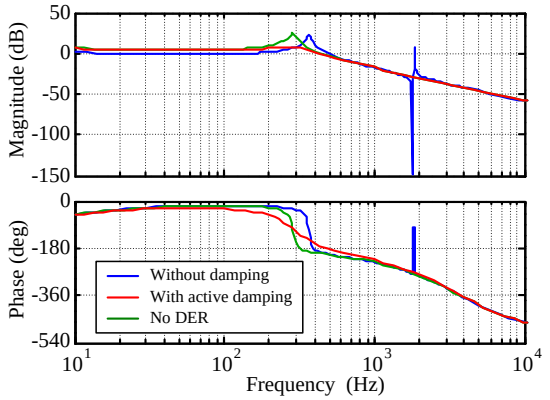

(a)

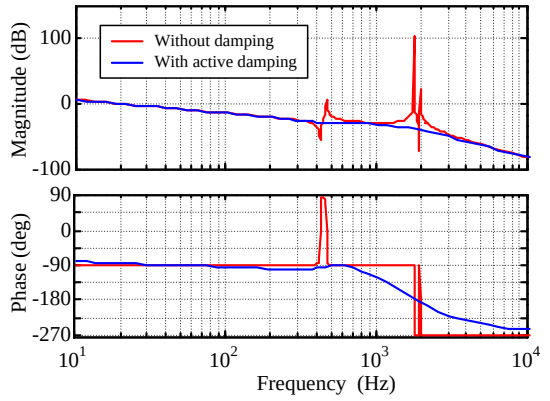

(b)

Fig. 7. Comparisons of open-loop Bode diagrams of diagonal elelments with/ without damping: (a) G_{11} and (b) G_{22}

The open-loop Bode diagrams of G_{22} are shown in Fig. 7(b). Compared with the Bode diagram without damping (red line), both the internal and external resonance peaks are completely attenuated by the active damping method as the blue line. The −180º crossings at the critical frequencies are cancelled within the whole range. More importantly, the amplitudes of the system are not reduced except the resonance points, guaranteeing the control performance of DERs.

TABLE I. CIRCUIT PARAMETERS

Symbol	Quantity	Value
L_{f1}	ST inverter inductance	5.2 mH
C_{f1}	ST inverter capacitance	60 μF
L_{ff}	DER inverter-side inductance	5.2 mH
L_{gf}	DER grid-side inductance	1.5 mH
C_f	DER inverter capacitance	6.8 μF

B. *Design of the Outer-Loop Control*

From the Bode diagrams shown in Fig. 4, we see that the external resonance of ST can be largely attenuated with the increasing of the DERs and line impedance, while those of DERs are not. On the other hand, since the capacitor value of ST is much larger than that of the DER. The ST introduces lower frequency external resonance to the DERs as it shown in Fig. 5. In this regard, the DERs are more sensitive to the external resonances as well as low-order harmonics.

With these considerations, the outer-loop control of ST and DER inverters utilize repetitive control (RC) and PR control, respectively. Fig. 8 shows the detailed control diagrams of the control systems of the ST and DER inverters. Both the RC and PR controllers can provide superior steady-state performance for sinusoidal signals. In addition, the RC can well eliminate the low-order harmonics and guarantee the ST LV side voltage with good power quality. In this way, the low-order harmonic propagation can be avoided within the microgrid and enhance its harmonic stability.

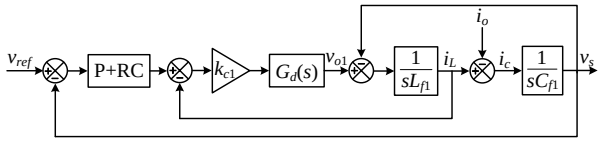

(a)

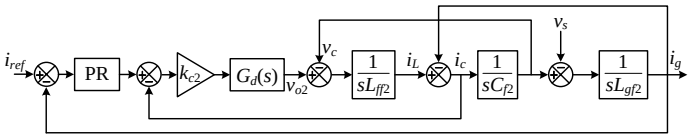

(b)

Fig. 8. Control diagrams of ST-based microgrid: (a) voltage control of ST inverter and (b) current control of DER inverter

As pointed out in Section III-A, phase lags are introduced by the active damping method. Therefore, necessary phase-lead elements shall be included in the outer-loop to compensate the phase lags. A phase-lead compensating term can be simply given as

$$G_f(j\omega) = e^{j\varphi(\omega)} \tag{11}$$

Specifically, in a digital system, the expression of G_f can be written as

$$G_f(z) = z^{N_1} = z^{\frac{\varphi(\omega)\cdot N}{2\pi}} \tag{12}$$

where N_1 is the leading phase steps and N is the sampling times per fundamental cycle, which can be expressed as $N = f_s / f$ with f_s and f being the sampling frequency and fundamental frequency. The leading phase of $\varphi(\omega)$ and N_1 of (10) can be easily determined by experiments in practical system. Considering the phase-lead elements, the expressions of resonant part (in PR control) and repetitive control can be given as followings

$$G_r = k_r \cdot \ell\{\sin(\omega t + \varphi)\} = k_r \cdot \{\frac{\cos\varphi \cdot s}{s^2 + \omega^2} + \frac{\sin\varphi \cdot \omega}{s^2 + \omega^2}\} \quad (13)$$

$$G_{rc} = k_{rc} \cdot \frac{z^{-N} \cdot G_f(z)}{1 - z^{-N}} \quad (14)$$

where ω is the fundamental frequency of the resonant controller.

C. Stability Analysis

Fig. 9(a) shows the stability (phase) margins and Nyquist plots of ST LV side inverter system with different inner-loop gains, where k_{c1} and k_{c2} are the inner-loop gains of ST and DER inverters, respectively. With the introduction of the inner-loop gains, the phase margins will gradually change from unstable region to stable region. In the stable region, the phase margins increase with the increasing of gains, meaning that the system becomes more stable. The Nyquist plots shown in Fig. 9(b) further confirm the conclusions. With proper damping gains, the system becomes stable because there is no encirclement of the point at (−1, *j*0). Similar conclusions can be drawn in the DER inverter case with these stability analyses. However, when inner-loop gains become high, there are considerable phase lags in low-frequency range which are bad for the waveform controls. So a trade-off of inner-loop gains should be made between the stability and the phase lags.

IV. Simulation and Experimental Results

A. Simulation Results

To validate the righteousness of the analysis as well as the effectiveness of the proposed control strategies, a ST-based microgrid was simulated by using the MATLAB/Simulink environment and the aid of the PLECS toolbox. In our study cases, four DER systems are connected to the PCC, whose voltage is supplied by a ST through the power line. The filter parameters of ST LV side inverter and DER inverters are same as those in Table I, the line impedance between ST LV side and PCC is 0.1+*j*0.15 Ω, and the detailed control parameters are listed in Table II.

Fig. 10 illustrates the simulated voltage profiles of the ST and output current of each DER when active damping method is not employed. Although the control parameters of each DER are properly designed, the results indicate that the integrated system is unstable. Amplified low-order harmonics propagate within the microgrid and leads to severe oscillations and distortions in the DER current. However, the voltage profile of ST is acceptable with relatively low THD (=3.15%), it proves the ST is less insensitive to the resonance as well as harmonics in such system. Fig. 11 shows the simulated waveforms when active damping method is used. It can be observed that both the ST LV side voltage and the DER current are much better than those of Fig. 10.

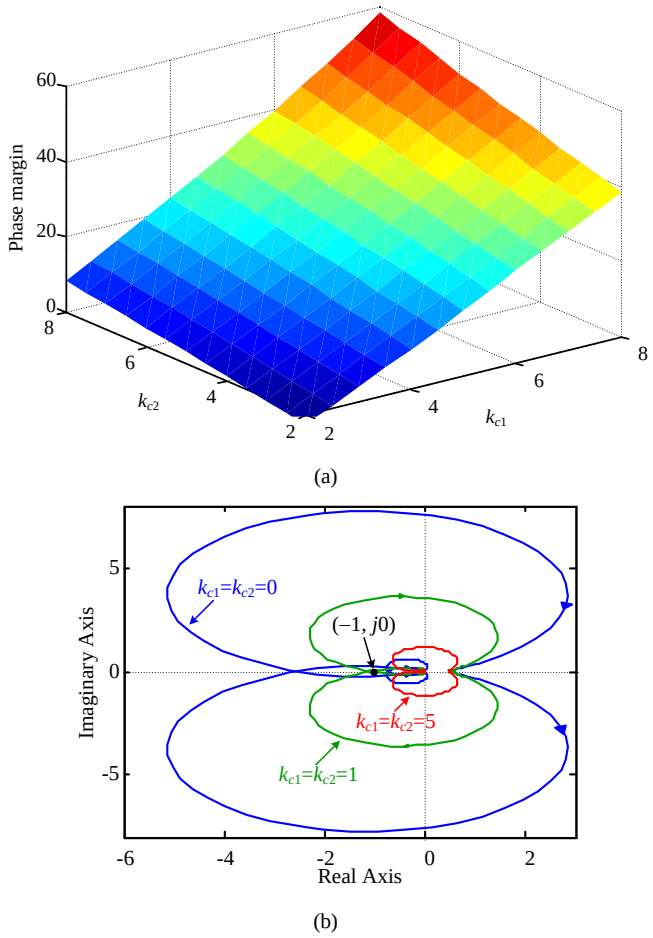

Fig. 9. Stability analysis of the ST-based microgrid with different inner-loop gains: (a) phase margins and (b) Nyquist plots

TABLE II. Control Parameters

Symbol	Quantity	Value
k_{pv}	Proportional gain of ST inverter	1.8
k_{rc}	Repetitive gain of ST inverter	0.15
k_{pi}	Proportional gain of DER inverter	2
k_r	Resonant gain of DER inverter	25
k_{c1}	Inner-loop gain of ST inverter	8
k_{c2}	Inner-loop gain of DER inverter	8

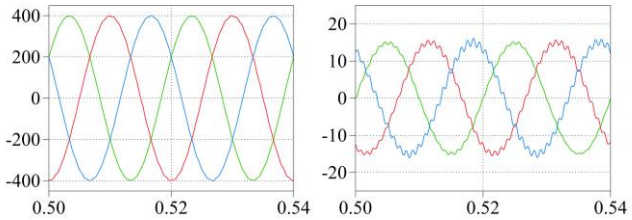

Fig. 10. Simulated performance of ST-based microgrid without active damping (x: time (s)): (a) ST voltage (y: voltage (V)) and (b) DER current (y: current (A))

The dynamic performance of the ST-based microgrid with the active damping method is also verified in the simulation. In this case, three DERs are connected to the PCC at first, and the 4th DER is plugged into the microgrid at *t*=0.2s. Fig. 12 shows the LV side voltage profile and current of the ST. It can be seen that the ST voltage is quite stiff during the connection

of DER, while the ST current can recover to its steady-state in less than one cycle. Moreover, because of the communication within the microgrid, the ST can instantly assign set-points to all the DERs. As a result, the RMS value of ST current before and after the transient point (t=0.2s) are almost the same. The DER currents at the transient state are shown in Fig. 13. All DERs present good dynamics during both the transient and the start-up.

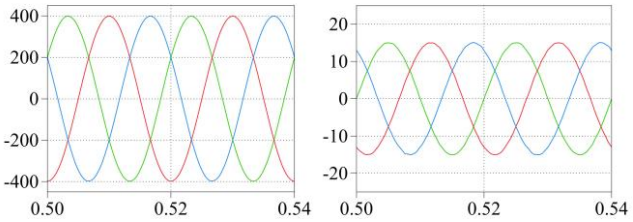

(a) (b)

Fig. 11. Simulated performance of ST-based microgrid with active damping (x: time (s)): (a) ST voltage (y: voltage (V)) and (b) DER current (y: current (A))

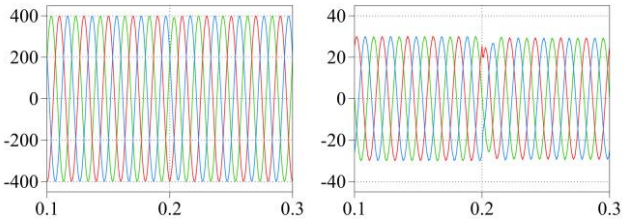

(a) (b)

Fig. 12. Dynamic performance of ST-based microgrid when one DER plugs into the system (x: time (s)): (a) ST voltage (y: voltage (V)) and (b) ST current (y: current (A))

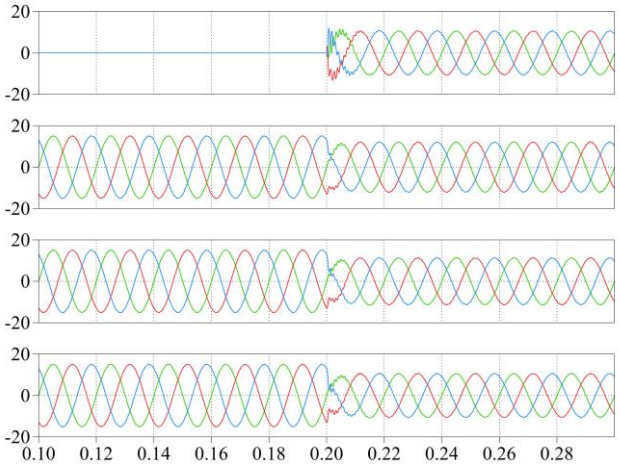

Fig. 13. DER currents of ST-based microgrid when one DER plugs into the system (x: time (s), y: current (A))

B. Experimental Results

To verify the effectiveness of this ST-based microgrid in a laboratory scale prototype, the laboratory setup with the same configuration and parameters of simulation is built, and its photograph is given in Fig. 14. The ST inverter uses a Semikron AN8005 IGBT inverter and is controlled by a dSPACE1104 control card. The DER inverter uses an IPM25RLA120 module and is controlled by a TMS320F2812.

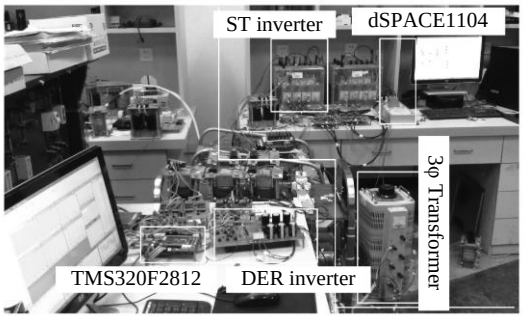

Fig. 14. Experimental setup

Fig. 15(a) shows the measured voltage of ST LV side inverter, and the corresponding THD value is 0.663%, which indicates the steady-state performance of ST inverter is quite good. With the voltage support of ST, the output current of the DER inverter is shown in Fig. 15(b) with the THD value being 2.239%. The results point out that a ST-based microgrid can provide high performance power quality within the whole system. The active damping adopted here ensures the system stability and largely alleviates the interactions between ST and DER.

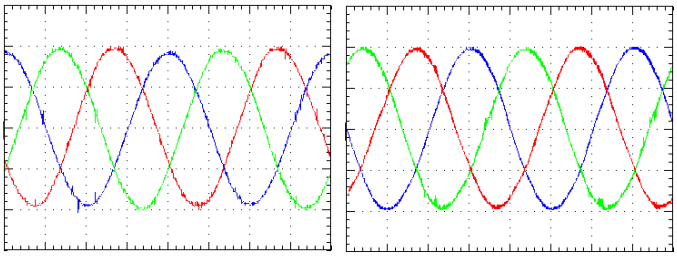

(a) (b)

Fig. 15. Measured steady-state waveforms (x: 5ms/div): (a) ST voltage profile (y: 150V/div) and (b) DER output current (y: 5A/div)

V. Conclusions

This paper presents a novel microgrid operated with a ST and discusses the resonance problem as well as stability issue of the system. A simplified system model and its two equivalent circuits have been presented to identify the potential resonances and analyze the interactions. To solve the problems, multiloop-based active damping methods have been adopted in both the ST and the DER inverters and the damping effects are well studied. The outer-loop control design for ST and DER inverters are also given in this paper. Simulation and experimental results verify the righteousness of our analysis and the effectiveness of the proposed control system.

References

[1] Fraunhofer Institute, "Electricity production from solar and wind in Germany in 2014," Germany, 2014.

[2] C.C. Chan, "The state of the art of electric and hybrid vehicles," *Proceedings of the IEEE*, vol. 90, no. 2, pp. 247-275, Feb. 2002.

[3] A. Bhowmik, A. Maitra, S.M. Halpin, and J.E. Schatz, "Determination of allowable penetration levels of distributed generation resources based

on harmonic limit considerations," *IEEE Trans. on Power Delivery*, vol. 18, no. 2, pp. 619-624, Apr. 2003.

[4] V.H.M. Quezada. J.R. Abbad, and T.G.S. Román, "Assessment of energy distribution losses for increasing penetration of distributed generation," *IEEE Trans. on Power Systems*, vol. 21, no. 2, pp. 533-540, May 2006.

[5] E.J. Coster, J.M.A. Myrzik, B. Kruimer, and W.L. Kling, "Integration issues of distributed generation in distribution grids," *Proceedings of the IEEE*, vol. 99, no. 1, pp. 28-39, Jan. 2011.

[6] H. Farhangi, "The path of the smart grid," *IEEE Power and Energy Magazine*, vol. 8, no. 1, pp. 18-28, Jan./Feb. 2010.

[7] A.Q. Huang, M.L. Crow, G.T. Heydt, J.P. Zheng, and S.J. Dale, "The future renewable electric energy delivery and management (FREEDM) system: The energy internet," *Proceedings of the IEEE*, vol. 99, no. 1, pp. 133-148, Jan. 2011.

[8] J.H.R. Enslin and P.J.M. Heskes, "Harmonic interaction between a large number of distributed power inverters and the distributed network," *IEEE Trans. on Power Electron.*, vol. 19, no. 6, pp. 1586–1593, Nov. 2004.

[9] J. Agorreta, M. Borrega, J. Lopez, and L. Marroyo, "Modeling and control of *N*-paralleled grid-connected inverters with LCL filters coupled due to grid impedance in PV plants," *IEEE Trans. on Power Electron.*, vol. 26, no. 3, pp. 770–785, Mar. 2011.

[10] J. He, Y.W. Li, D. Bosnjak, and B. Harris, "Investigation and active damping of multiple resonances in a parallel-inverter-based microgrid," *IEEE Trans. on Power Electron.*, vol. 28, no. 1, pp. 234–246, Jan. 2013.

[11] X. Wang, F. Blaabjerg, and W. Wu, "Modeling and analysis of harmonic stability in an AC power-electronics-based power system," *IEEE Trans. on Power Electron.*, vol. 29, no. 12, pp. 6421–6432, Dec. 2014.

[12] R. Pena-Alzola, G. Gohil, L. Mathe, M. Liserre, and F. Blaabjerg, "Review of modular power converters solutions for smart transformer in distribution system," in *IEEE 2013 Energy Conversion Congress and Exposition*, 2013, pp. 380-387.

[13] K. Christakou, J. LeBoudec, M. Paolone, and D.C. Tomozei, "Efficient computation of sensitivity coefficients of node voltages and line currents in unbalanced radial electrical distribution networks" *IEEE Trans. on Smart Grid*, vol. 4, no. 2, pp. 741-750, Jun. 2013.

[14] G.D. Carne, M. Liserre, K. Christakou, and M. Paolone, "Integrated voltage control and line congestion management in Active Distribution Networks by means of smart transformers," *IEEE International Symposium on Industrial Electronics (ISIE)*, pp. 2613-2619, Jun. 2014.

[15] Y.W. Li, "Control and resonance damping of voltage-source and current-source converters with *LC* filters," *IEEE Trans. on Ind. Electron.*, vol. 56, no. 5, pp. 1511–1521, May 2009.

[16] J. Dannehl, M. Liserre, and F.W. Fuchs, "Filter-based active damping of voltage source converters with *LCL* filter," *IEEE Trans. on Ind. Electron.*, vol. 58, no. 8, pp. 3623–3633, Aug. 2011.